International Journal of Biological Macromolecules 257 (2024) 128598

Contents lists available at ScienceDirect

International Journal of Biological Macromolecules

journal homepage: www.elsevier.com/locate/ijbiomac

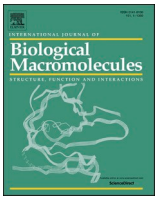

Fabrication of chitosan/fibrin-armored multifunctional silver nanocomposites to improve antibacterial and wound healing activities

Anandhavelu Sanmugam [a], D. Shanthi [b], Ananda Babu Sairam [a], Raju Suresh Kumar [c], Abdulrahman I. Almansour [c], Natrajan Arumugam [c], A. Kavitha [d], Hyun-Seok Kim [e], Dhanasekaran Vikraman [e,*]

[a] Department of Applied Chemistry, Sri Venkateswara College of Engineering, Sriperumbudur 602117, India
[b] Department of Chemistry, Vel Tech Multi Tech Dr.Rangarajan Dr.Sakunthala Engineering College, Avadi, Chennai 600062, TamilNadu, India
[c] Department of Chemistry, College of Science, King Saud University, Riyadh 1451, Saudi Arabia
[d] Department of Chemistry, Chennai Institute of Technology, Sarathy Nagar, Kundrathur, Chennai 600069, TamilNadu, India
[e] Division of Electronics and Electrical Engineering, Dongguk University-Seoul, Seoul 04620, Republic of Korea

ARTICLE INFO

Keywords:
Chitosan
Antibacterial
Wound healing

ABSTRACT

A wound healing substitute promotes rapid tissue regeneration and protects wound sites from microbial contamination. The silver-based antiseptic frequently moist skin stains, burns and irritation, penetrates deep wounds and protects against pathogenic infections. Thus, we formulated a novel fibrin/chitosan encapsulated silver nanoparticle (CH:F:SPG-CH:SNP) composites bandage accelerating the polymicrobial wound healing. Electrospinning method was employed to form the nano-porous, inexpensive, and biocompatible smart bandages. The structural, functional, and mechanical properties were analyzed for the prepared composites. The biological capacity of prepared CH:F:SPG-CH:SNP bandage was assessed against NIH-3 T3 fibroblast and HaCaT cell lines. *In vitro* hemolytic assays using red blood cells were extensively studied and explored the low hemolytic effect (4.5 %). In addition, the improved drug delivery nature captured for the CH:F:SPG-CH:SNP composite bandage. Antibacterial experiments were achieved against *Pseudomonas aeruginosa*, *Escherichia coli*, *Staphylococcus aureus* and *Lactobacillus bulgaricus* using zone inhibition method. Moreover, *in-vivo* wound healing efficacy of fabricated smart bandage was evaluated on the albino Wistar rats which revealed the significant improvement on the postoperative abdomen wounds.

1. Introduction

Standardized drug delivery procedures are inevitable to deliver the medications over a prolonged span with the least side effects. [1,2] These practices can offer the equal efficacy from the biological and synthetic substances. [3,4] The various traditional and modern wound healing application medications were used for tissue replacement, particularly dermis damage on the wound site. In the advanced smart dressing applications, 'smart polymers' are used by the modifications of synthetic and natural biopolymers. [5,6] Many developments are in progress to develop a new generation skin wound substitute especially for the postoperative abdomen wound closure. [7,8] These cases mostly bioactive polymers replace the lost tissue instead of facilitating wound healing from the synthetic form which are able to mimic normal physiological responses during tissue granulation. [9–11] The use of topical agents with biopolymers possess cleansing and debridement, which always possess antimicrobial, antiseptic and antibacterial effects. [12,13] In a new generation smart wound dressing, the nanoparticles are given the significant therapeutic role by the prevention infection growth and aid to support the tissue regeneration. [14] Many research reports describe smart polymers with nanoparticles can provide tissue compatibility, degradability, controlled drug release, swelling ability and nanoporous structure. [6,15–17]

A natural biopolymer of chitosan (CH) is given the extensive properties such as soft adhesive, biocompatible, biodegradable, hemostatic and antibacterial. [10,18] Chitosan is a composition of β-(1.4)-2-acetamido-2-deoxyglucopy-ranose and 2-amino-2-deoxyglucopyranose units. [19–21] Moreover, its biological properties and hydrophilic functions widely used for faster wound healing. The bacteriostatic and fungi static properties initiate cell proliferation and tissue organization

* Corresponding author.
E-mail address: v.j.dhanasekaran@gmail.com (D. Vikraman).

https://doi.org/10.1016/j.ijbiomac.2023.128598
Received 28 August 2023; Received in revised form 1 December 2023; Accepted 2 December 2023
Available online 4 December 2023

particularly useful in chronic wounds. [22] The formation of chitosan has been a proven candidate for delivering peptides, proteins and plasmids, and its ability to release controlled drug due to hydrophilicity and cross-linking density. [23,24] The plentiful available shrimp shells are used to develop chitosan nanoparticles which is showing the effective medical importance against insecticides. [25] Recently, Packirisamy et al. [26] have prepared the chitosan formulated zinc stannate for the antibacterial activity against *E. coli*, *S. typhi* and *K. pneumoniae* species. In addition, reduced graphene oxide/Fe_3O_4/chitosan nanocomposites showed enhanced cytocompatibility nature against A549 and MCF7 cell lines and *S. aureus*, *P. aureginosa* and *C. albicans* pathogens. [27] The use of silver nanoparticles have gained much attention and exhibited improved antibacterial activities when compared to bulk silver. These nature can be induced by the large fraction of surface atoms and high surface area where more amount of nanoparticles insertion towards the bacteria and boosting their ability in a prolonged way. [14,28] The nature of chitosan at low aqueous solubility medium tends to be an effective biomaterial to absorb large volume of exudates/water. [29] A balance chitosan loading factors with other biopolymers such as polymer ratio, solubility, temperature and pH enhances wound healing and facilitates tissue growth. [30] Recently, chitosan/agar-silver nanoparticles coated paper have shown improved antibacterial performance *versus* the gram-positive and gram-negative bacterial species. [31]

Fibrin (F) is a natural protein and an important component of blood to initiate blood clot. It possesses cellular attachment, cell proliferation and extracellular matrix formation for hemostasis and wound healing applications. [32,33] It is an excellent biopolymer with biocompatible and biodegradable properties hence tissue regeneration can be achieved in shorter time. Fibrin reported as a potential drug delivery polymer to release sustainable amount of drug and proteins at damaged tissue site. [34] During the surgical suture procedures, the fibrin glue and fibrin gel could be used to provide slow delivery of antibiotics to expose on tissue. [35] Fibrin based scaffolds exhibit excellent growth aspect deliveries such as fibroblast growth factor and vascular growth factor. However, fibrin incorporated drug and polymers can be easily injected for local deliver at desired wound site. [36]

Silver nanoparticles (SNP) are specifically influential candidates for the various fields due to their stunning behaviors such as optical characteristics, electrical conductivity, and chemical stability. [37–39] SNPs are possible to hinder the growth of various pathogens by distinguished mechanisms, including ROS production, DNA spoil, membrane impairment, intracellular proteins inactivation and so on. [40,41] SNP nanoparticles are having the wide range of pharmaceutical uses, including tissue engineering, drugs delivery, and pathogens sensor. [42] However, the unnecessary toxic materials absorbance on the surface of SNPs could be created toxicity and limitation towards their use for clinical purposes. [40] In recent time, electrospinning preparation is a highly attractive and economical procedure to manufacture the various nano and submicron polymeric frameworks. [43,44]

In this study, a facile electrospinning method was applied to progress a macroporous chitosan/fibrin/silver nanoparticles based smart bandage (CH:F:SPG-CH:SNP) where the SNP was impregnated *via* electrospinning to fabricate a potential abdominal wound substitute. As a functional wound dressing, chitosan and fibrin scaffold can be achieved through various matrix ratios. In addition, chitosan wound dressing has many adhesive and antimicrobial properties, as well as fibrin also have hemostatic sealant properties. The prepared bilayer scaffold of CH:F:SPG-CH:SNP smart bandage would be a biomimetic material to absorb wound exudates for rapid healing of abdominal wounds. Thus, this work is focused on forming the smart bandage using biopolymers with macro porous structure and its efficacy for would healing was evaluated using *in vitro* and *in vivo* studies. In addition, the antibacterial properties against the *P. aeruginosa*, *E. coli*, *S. aureus* and *L. bulgaricus* using zone inhibition procedures. The mupirocin drug delivery and hemolytic effects were analyzed for the fabricated smart bandage.

2. Materials and methods

2.1. Preparation of fibrin from bovine source

The commercially availed blood source form the slaughter house was routinely blended with glass rod to extract fibrin. [45] Then, the naturally obtained fibrin was cleansed to remove the blood clots under running water. Further, the extracted fibrin was cured with hydrogen peroxide solution (25 %) and sodium acetate solution (0.5 M). Finally, the cleansed fibrin was washed under pouring water and lyophilized, then stored at room temperature for analysis.

2.2. Fabrication of chitosan/fibrin sponge

Initially, chitosan was obtained from the earlier described procedure. [46] An aqueous chitosan was equipped with 1 % acetic acid using an as-prepared material. A neutral pH was maintained for equipped solution and then centrifugation process was carried out to remove the leftover water and residues. Lastly, magnetic stirring was employed at room temperature for 5 h for the homogeneous mix of resultant chitosan solution. Then, two different ratios (weight percentage) of as-prepared fibrin in terms of chitosan such as 1:1 and 1:2 were dissolved using water and subsequently blended with chitosan solution using homogenizer at 20000 rpm at 4 °C for 15 min. Later, 5 drops of ethylene glycerol were added as cross-linker after 20 mins of magnetic stirring. Finally, the homogenous mixture was transferred into Teflon template followed by deep freezing at −20 °C for 14 h. The resulting chitosan/fibrin sponge material was lyophilized and denoted further as CH/F.

2.3. Electrospinning of nanofibrous bilayer matrix

The homogenous chitosan solutions were equipped in room temperature by mixing 2 g of as-prepared chitosan in acetic acid with magnetic rousing for 10 h. Followed by SNP's were poured into CH solutions at constant rousing for 8 h and obtained a uniformly distributed CH:SNP. The uniformly blended solution were electrospun over the fabricated sponge form of CH:F:SPG positioned on the rectangular aluminum substrate with a separation of 14 cm^{-1} perpendicular to the 24G needle linked to positive terminal of power supply. [47] Using a syringe pump with controlled electric potential of 1.5 kV/cm, the blended drug polymer solution was squeezed out. After complete dehydration of the drug polymer solvent from the CH:F:SPG-CH:SNP bandage to make the bilayer nanofibrous matrices. Moreover, the equipped bandages were kept at room temperature for further use.

2.4. Characterizations

Fourier transform infrared (FTIR, JASCO spectrophotometer), X'Pert PROPANalytical X-ray diffraction (XRD), field emission scanning electron microscope (FESEM, Carl Zeiss AG, Jena, Germany) and transmission electron microscope (TEM, FEI Tecnai G2, F30) measurements were used to determine the physio-chemical changes of chitosan, fibrin, and CH:F:SPG-CH:SNP materials.

2.5. Antimicrobial activity

Well diffusion method was employed to assess the antimicrobial activity of CH:F:SPG-CH:SNP with sterile Mueller Hinton Agar (MHA) media. The selected pathogens of *P. aeruginosa*, *E. coli*, *S. aureus* and L. *bulgaricus* were wiped onto the surface of MHA medium. The prepared bandage of CH:F:SPG-CH:SNP with various amount was placed on every part of well. Next, MHA plates were cultured at 37 °C for 24 h with ambient conditions.

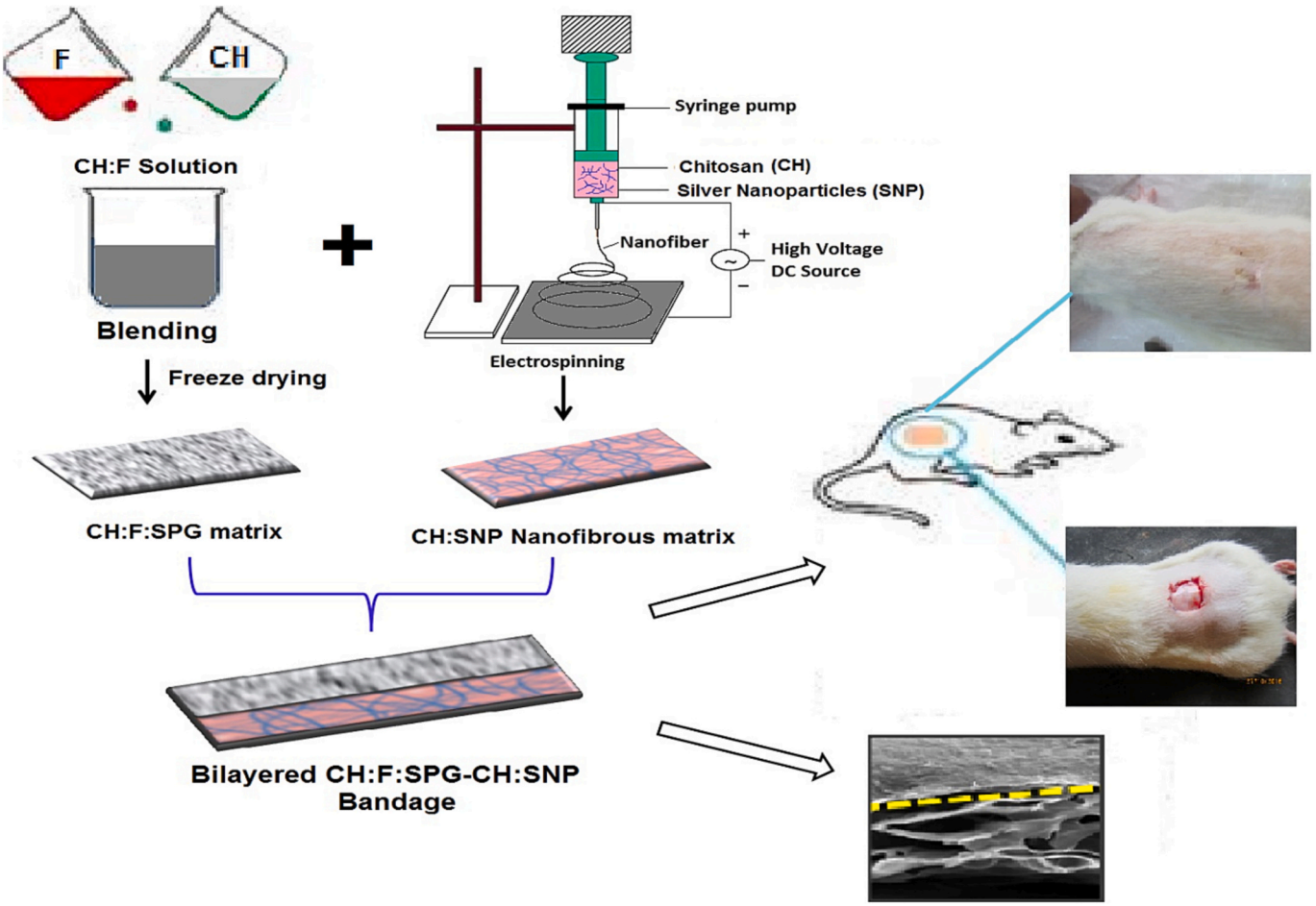

Scheme 1. Scheme for preparation of bilayer CH:F:SPG-CH:SNP bandage for wound healing

2.6. *In vitro* biocompatibility examination of bilayer sponge

The prepared bilayer sponge *in vitro* biocompatibility for the human keratinocytes (HaCaT) and NIH-3 T3 fibroblast cell lines were assessed by MTT assay. The cells were cultivated with Dulbecco's modified eagle medium (DMEM) over CH-SPG, CH-SPG:GE and CH-SPG:GE-SNP bilayer sponge in 24 wells plate for 1, 3 and 5 h. The fetal calf serum was maintained at 37 °C and inserted with 2 mg/mL amphotericin B, 150 mg/mL gentamycin 60 mg/mL streptomycin and 100 U/mL penicillin. Then, 100 μL of blended was shifted to culture growth plate. A control sample was grown without bilayer bandage. Universal microplate reader at 570 nm was employed to measure the solution absorbance. After the broth culture, the medium was detached and washed with phosphate buffer saline (PBS) to calculate the cell formation and morphology on the bilayer bandage. Fluorescence staining technique was employed to envision the *in vitro* cell propagation on the culture of bilayer bandage at various intervals 1, 3 and 5 h. Phase contrast microscopy was employed to visualize the nuclei and living cells after the counterstaining process using DAPI (2 mg/mL) and Calcein AM (2 μM) with the 37 °C incubation for 30 mins on the stained cells. [48]

2.7. *In vitro* hemocompatibility assay

Hemolysis assay is essentially resulted by the osmotic pressure increment on the red blood cells (RBCs). The occurrence of division followed by the release of hemoglobin on the RBCs was observed during hemolysis. A hemolytic assay was engaged to realize the blood coordination of the CH:F:SPG-CH:SNP framework on human RBCs. The blood samples were collected from the volunteer and then a human RBCs suspension of 15 % *v*/v was prepared in 0.9 % NaCl. Subsequently, determined pieces of fibrin, chitosan or CH:F:SPG-CH:SNP framework (4 mm × 4 mm) was sited, and suspension (100 μL) was dropped in each well of 96-well plate. Also, 0.9 % sterile NaCl solution and 1 % Triton X-100 solution was engaged as a negative and positive control, respectively for 100 % lysis of erythrocytes. [49] In this test, each treatment was repeated three times. Further, the 96-well inoculation was incubated for 1 h at 37 °C and then centrifugated at 3500 rpm for 10 min. To evaluate the absorbance, the supernatant (150 μL) was placed on a new 96-well plate using a microplate reader (STAT FAX 2100, BioTek) with 414 nm. Finally, the percentage of hemolysis was derived using the ensuing Eq. (1).

$$\text{Hemolysis}\% = \left(\frac{mean\ OD\ of\ sample – mean\ OD\ of\ negative\ sample)}{mean\ OD\ of\ positive\ control - mean\ OD\ of\ negative\ control}\right) \times 100 \quad (1)$$

2.8. *In vivo* wound healing study

A male Albino Wister rats (220 to 275 g) were engaged for wound healing *in vivo* studies. They were watched and given the standard feed frequently in a 12 h light/dark cycle at 25 °C. The CH:F:SPG and CH:F:SPG-CH:SNP wound dressing bandage were employed to assess their wound healing efficacy on rats. Intra peritoneal injection of thiopentone sodium was used for anesthetizing rats with a dose of 50 mg/kg body weight. To shave dorsal region of skin, an antiseptic encompassing 70 % alcohol was employed. On the animal model a full thickness cutting out wound was made with the size of 2 × 2 cm^{-2}. For this examination, 48

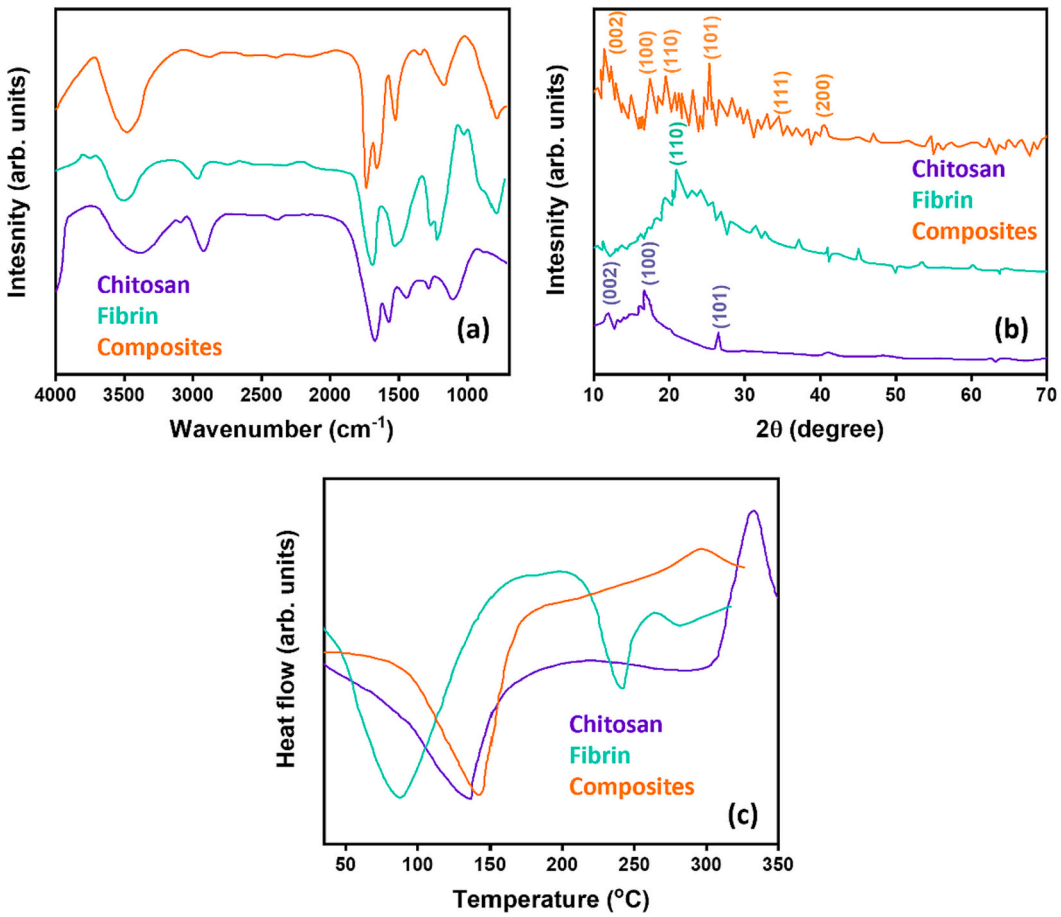

Fig. 1. (a) FTIR, (b) XRD and (c) TG-DTA spectra of fibrin, chitosan, and (c) CH:F:SPG-CH:SNP.

rats were parted into three sections with sixteen rats in each section (Control, CH:F:SPG and CH:F:SPG-CH:SNP bandage). A sterile gauze was engaged for control section whereas CH:F:SPG and CH:F:SPG-CH: SNP bandage was used for Sections 2 and 3, respectively at the wound place. Ethylene oxide was used to sterile the sponge samples before dressing and the wound dressing was altered regularly. Continually at an interval of 4, 8 and 12 days, four rats from every section were forfeited and the granulation tissues were collected from them for regular histological protocols of staining. The wound healing development in all the sections of rats were assessed regularly on the wound surface for wound closure, histological and biochemical evaluation. [34]

2.9. Drug release experiments

The drug (mupirocin) discharge by the CH:F:SPG-CH:SNP nanoparticles was recognized at 37 °C using a Franz-type cell. The recipient element was supplied with PBS (pH = 7.4) under 1 h of constant stirring. Then, the supernatant solution was removed using centrifugation from the obtained buffer by recipient. The drug substance ratio was defined from the rest by determining the absorbance (Shimadzu ultraviolet spectrometer). [50] The drug out percentage from CH:F:SPG-CH:SNP nanoparticles was estimated as follows.

$$E = Q_p/Q_t \text{ x } 100 \quad (2)$$

where Qt is the total quantity of drug merged with the nanoparticles, Qp is the released drug quantity, and E is the drug release percentage from CH: F: SPG-CH:SNP nanoparticles.

2.10. Statistical analysis

All the measurements were presented as mean ± standard deviation ($n = 3$). The statistics were performed using ANOVA (Analysis of Variance) and student's *t*-test was completed to calculate the significant variances between the set of results. The stated variations were statistically significant when $p < 0.05$.

3. Results and discussion

3.1. Chemical and structural characterizations

CH:F:SPG-CH:SNP framework was assembled using the electrospinning of silver nanoparticles as shown in Scheme 1. Further, functional properties were derived by the FTIR, XRD and thermogram results for the chitin, fibrin and CH:F:SPG-CH:SNP. Fig. 1(a) shows the FT-IR spectra of chitin, fibrin and CH:F:SPG-CH:SNP. The characteristic bands of both chitosan and fibrin are accumulatively observed in the bilayer nanofibrous matrices. The broad band around 3500–3400 cm^{-1} may be attributed to the–OH and $–NH_2$ stretching vibrations of chitosan. [51,52] The peak at 1029 cm^{-1} may be due to the saccharide structure of chitosan. [26] The peaks at 1639, 1564 and 1417 cm^{-1} corresponds to the amide I (C—O), amide II (C—N and N—H) and amide III (C—N) vibrations from fibrin, respectively. [53]

Fig. 1(b) shows the X-ray diffraction pattern of chitosan, fibrin and CH:F:SPG-CH:SNP. The broad diffraction peaks at around 11.8° (002), 16.6° (100) and 26.4° (101) of 2θ represent the characteristic peaks of chitosan. [39,40] The diffractogram of fibrin shows a broad diffractive peak located at around 20° (110). When compared with the pure form of chitosan and fibrin, the X-ray diffractogram of CH:F:SPG-CH:SNP shows

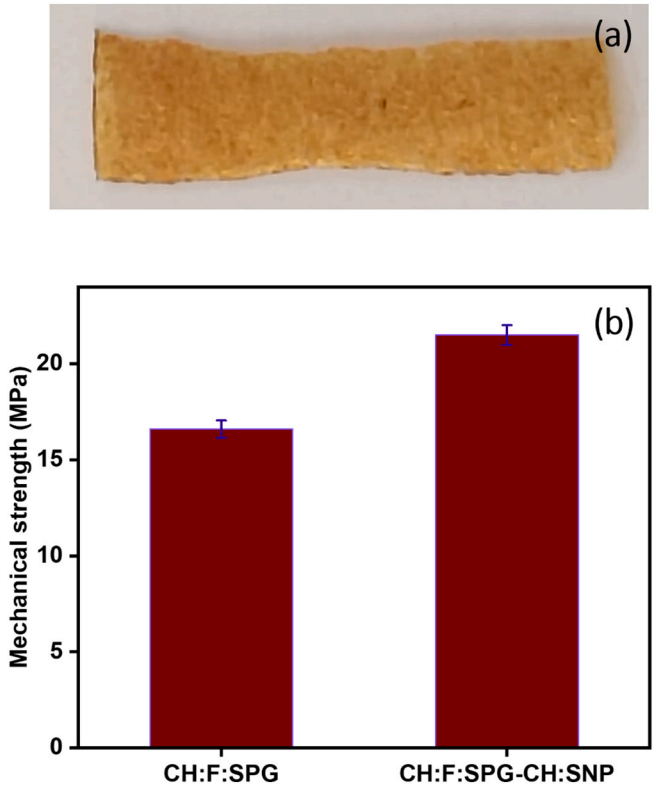

Fig. 2. (a) Photographic image of CH:F:SPG-CH:SNP bandage; (b) mechanical properties of CH:F:SPG and CH:F:SPG-CH:SNP.

certain changes in both the diffraction angles and peak intensity. The peak angle at around 10.5° has been shifted to a higher 2θ value of around 11.6° with no significant difference in the peak at around 20°. In addition, the peak related SNP is emerged at 34.3° (111) and 41.1° (200) in the CH:F:SPG-CH:SNP composites.

Thermograms of chitosan, fibrin, and CH:F:SPG-CH:SNP are shown in Fig. 1(c). An initial weight loss of about 9.5, 13, and 9 % was observed near 100 °C, which is credited to the evaporation of adsorbed water molecules present in chitosan, fibrin, and CH:F:SPG-CH:SNP respectively. A drastic decomposition of all the three samples was observed between 220 and 400 °C, which may be due to the degradation and depolymerization of saccharide rings and amino acid units of chitosan and fibrin. However, the weight loss slowed down after 400 °C and a total weight loss of about 69, 77, and 68 % was observed in chitosan, fibrin, and CH:F:SPG-CH:SNP, respectively at 600 °C. When compared with the pure form of fibrin, CH:F:SPG-CH:SNP show increased thermal stability, which may be because of the relations between the amino and carboxyl groups of chitosan and fibrin.

DSC results show an initial endothermic peak at 117 °C, 91 °C, and 142 °C, which is assigned to the loss of water molecules present in chitosan, fibrin, and CH:F:SPG-CH:SNP, respectively. Exothermic peaks at 317 °C and 283 °C, represent the decomposition of chitosan and CH:F:SPG-CH:SNP whereas the endothermic peak at 225 °C represents the decomposition of fibrin. This clearly indicates that chitosan-grafted fibrin nanocomposite shows relatively higher thermal stability when compared with the pure form of fibrin. Fig. 2(a) shows the photographic image of prepared CH:F:SPG-CH:SNP scaffold bandage. Exceptional mechanical characteristics are necessary to use attractive wound healing bandage to maintain reliability and shield the wounded region from the various exterior weights. [54] Fig. 2(b) shows the mechanical strength variations for the CH:F:SPG and CH:F:SPG-CH:SNP composite bandages to establish the stretchability properties. The results showed that the SA wound dressing ruptured easily at small loads strains of 2.351 N. CH:F:SPG-CH:SNP produces the maximum mechanical strength compared to their counterpart CH:F:SPG bandage which is due to the inclusion of chitosan bounded SNP. The observed performance was more consistent with reported literatures to equalize the wound dressing characteristics. [55]

FESEM and TEM analysis was done for the CH:F:SPG-CH:SNP scaffold. Fig. 3(a) shows the FESEM image which defines the well-ordered spherical shaped bilayer nanofibrous structure. Some of the nanoparticles were agglomerated because of their small size and high specific surface energy. Fig. 3(b) displays the TEM images of CH:F:SPG-CH:SNP composites. The observed results accumulated grains due to the coalescence process in the derived composites. Large area TEM image (inset Fig. 3(b)) clearly displays the agglomerated composite structure. The removal of toxic compounds and diffusion of nutrients are allowed by the porous structure. To determine the porous structure, nitrogen

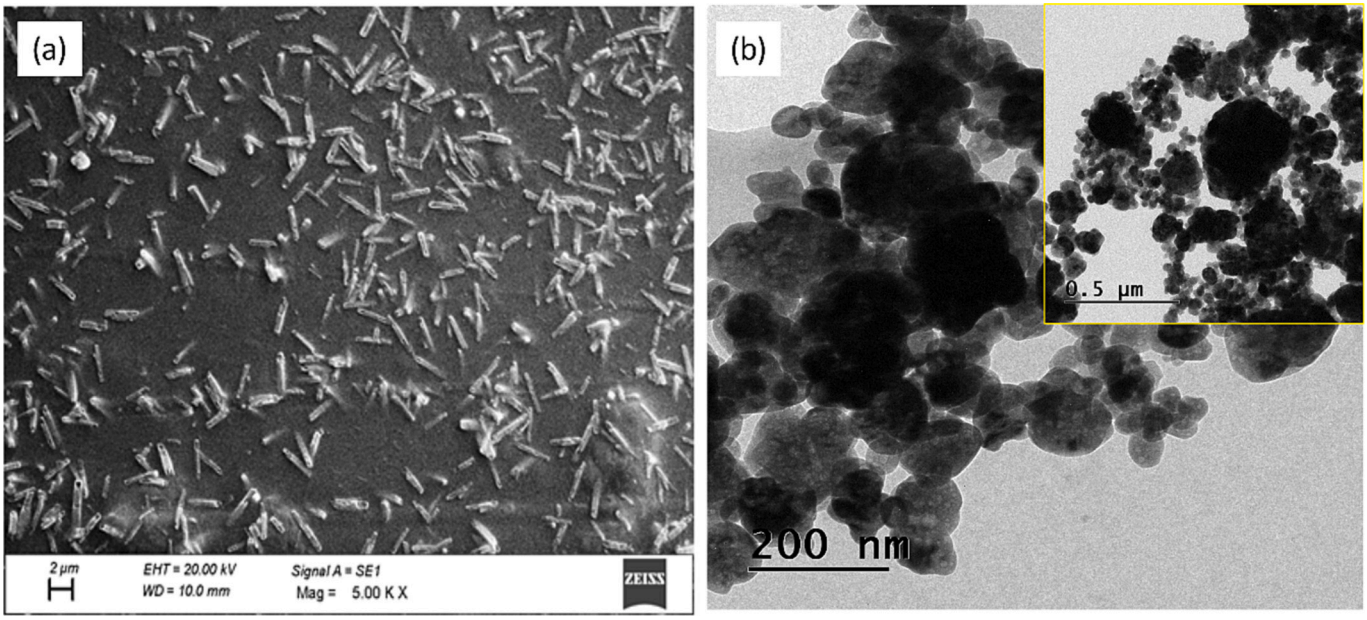

Fig. 3. (a) FESEM and (b) TEM images (inset: low magnification) of CH:F:SPG-CH:SNP.

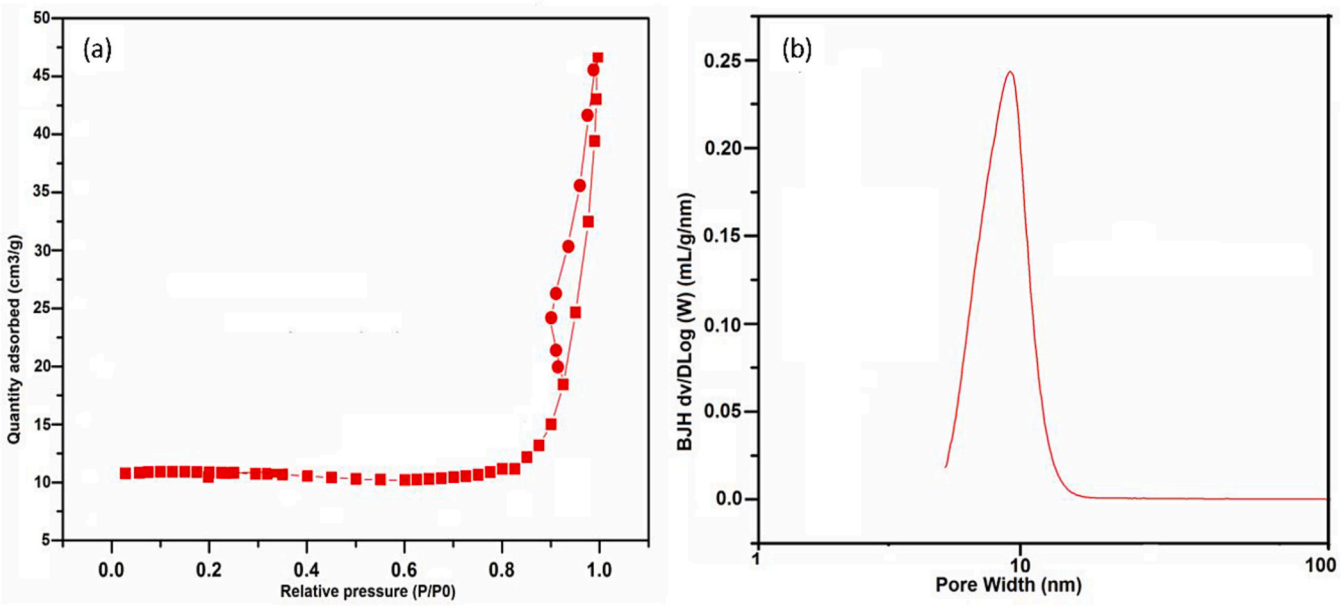

Fig. 4. (a) BET and (b) BJH profiles of CH:F:SPG-CH:SNP.

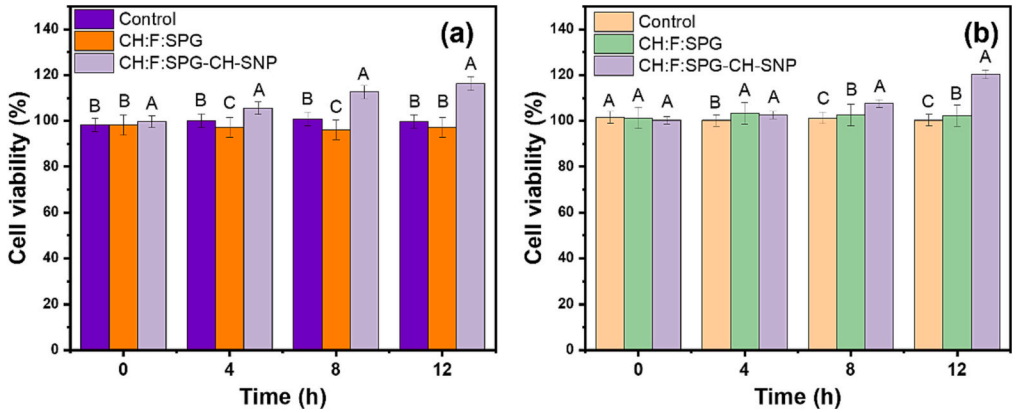

Fig. 5. MTT assay for the (a) Human keratinocytes (HaCaT) and (b) NIH-3 T3 fibroblast cell lines using CH:F:SPG-CH:SNP for the different time interval. The error values are provided from the standard deviation of replicated experiments. Capital alphabets denote a significant deviation between the replicated experiments ($P \leq 0.05$).

isotherm analysis was performed for CH:F:SPG-CH:SNP. Fig. 4(a-b) shows the BET and BJH spectrum of derived material, respectively. The measured result indicates the chitosan-grafted fibrin nanocomposite owned maximum porous structure with an average pore radius of~ 10 nm. This result demonstrates the large surface area of CH:F:SPG-CH:SNP which leads to good sorption ability.

3.2. *In vitro* biocompatibility studies

Smart wound dressing bandage with enhanced cell adhesion and cell proliferation properties are the crucial aspects in tissue regenerative activity. *In vitro* biocompatibility of CH:F:SPG and CH:F:SPG-CH:SNP bilayered bandage were assessed for HaCaT and NIH-3 T3 fibroblast cells at various time intervals by MTT assay as shown in Fig. 5(a-b), respectively. The cells were planted over nanoporous sponge layer which exhibited improved cell viability for both cell lines. The CH:F:SPG sponge produces lower cell viability than CH:F:SPG-CH:SNP bandage. The presence of silver nanoparticles in the nanofibrous bandage enhances the growth in the CH:F:SPG-CH:SNP bilayer bandage. In addition, chitosan attracts the fibroblast cells effectively on their walls which induces the significant increment of cell viability. Due to the availability of high porous sponge attached with well-designed silver nanoparticles in the CH:F:SPG-CH:SNP nanofibrous structure, the cell and cell proliferation are well established. Also, the interaction between the CH:SNP and CH:F:SPG helps to achieve improved cell bonding and movement. The fibrin increases adhesive property and sustained release of nano drug and proteins. Further, the silver nanoparticles help to block the burning and inflammation sensation at the wounded area. Finally, the studied *in vitro* outcomes reveal the cyto-compatible behavior of CH:F:SPG-CH:SNP. *In vitro* fluorescent staining performance with Calcein and DAPI for the bilayer bandages was estimated using NIH-3 T3 fibroblast and HaCaT cell lines after 12 h. The obtained results explored that compatibility of prepared biocomposite bandages not only assisted the penetration of cells into the tissue inner layer but also improved the nutrients and oxygen transfer to the cells.

3.3. *In vitro* hemocompatibility results

Hemocompatibility is a highly considerable reason to decide the use of transplantable materials. When the blood contacts with an external biomaterial, the primary process that happen is the competitive absorption of plasma proteins. [56] As per the ISO model, a <5 % of

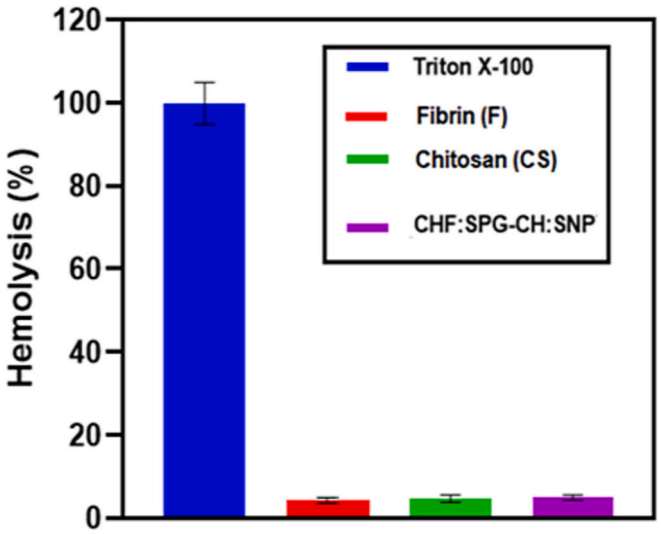

Fig. 6. Hemolysis histogram of fibrin, chitosan and CH:F:SPG-CH:SNP. The error values are provided from the standard deviation of replicated experiments.

hemolysis index is indicated as safe substance. [57] The hemolytic assay of CH:F:SPG-CH:SNP bandage for the human erythrocytes was assessed to verify its hemolysis strength (Fig. 6). The obtained results revealed that the CH:F:SPG-CH:SNP nanocomposite owns 4.5 % of hemolytic efficacy while the positive control sample of Triton X-100 lysed 95.7 % of RBCs. The pure form of fibrin and chitosan exposed the hemolytic activity of about 3.6 and 4 %, respectively for the comparison. Based on the observed results, CH:F:SPG-CH:SNP framework is compatible with blood cells and would be the suitable materials for wound healing and tissue engineering.

3.4. In vitro antibacterial results

Antibacterial efficacy of synthesized CH:F:SPG matrix, CH-SNPs and bilayered CH:F:SPG-CH:SNP nanocomposites were accomplished against *P. aeruginosa, E. coli, S. aureus* and L. *bulgaricus* bacteria. Fig. 7 shows the antibacterial activity of CH:F:SPG-CH:SNP in terms of zone of inhibition against *P. aeruginosa, E. coli, S. aureus* and *L. bulgaricus* pathogens. Streptomycin was used as the standard antibacterial agent. The observed well plated indicated the high inhibiting behavior against L. *bulgaricus* pathogen. However, other pathogens are considerably killed by the prepared bandage. The amount of bandage is significantly caused by the increment of zone of inhibition as resulted in Fig. 7. From the observed results, CH:F:SPG-CH:SNP nanocomposites are highly capable of immune the growth of L. *bulgaricus* effectively. Chelation processes of complexes are highly capable of changing the metabolic kinetics of pathogens to deactivate the cellular enzymes.

3.5. In vivo wound closure studies

Wound healing properties of three sections of animals were investigated using Albino Wistar rats (Control, CH:F:SPG and CH:F:SPG-CH:SNP). Fig. 8(a) illustrates macroscopic observations of *in vivo* wound closure treatment of the prepared composited materials in different post-surgery regions on 0, 3, 6 and 12th days. The experimental results show virtually completed (≈ 97 %) wound closure on 12th day with treatment of prepared CH:F:SPG-CH:SNP bandage materials when compared to the CH:F:SPG (86 %) and control (62 %) wound models as shown in Fig. 8 (b). But in SNP loaded bandage, the wound healing process is accelerated for fibroblast cell lines within the short duration. The assembled new bandage improves new tissue restoration and initiates re-ephithelialization owing to the distribution of substantial levels of protein at the wound site. In addition, SNP particles are also valuable for epithelial cell relations which are capable of emitting growth elements for epithelialization. Besides, the treatment of prepared bandage materials was exhibited fresh skin regeneration evenly in the absence of scars,

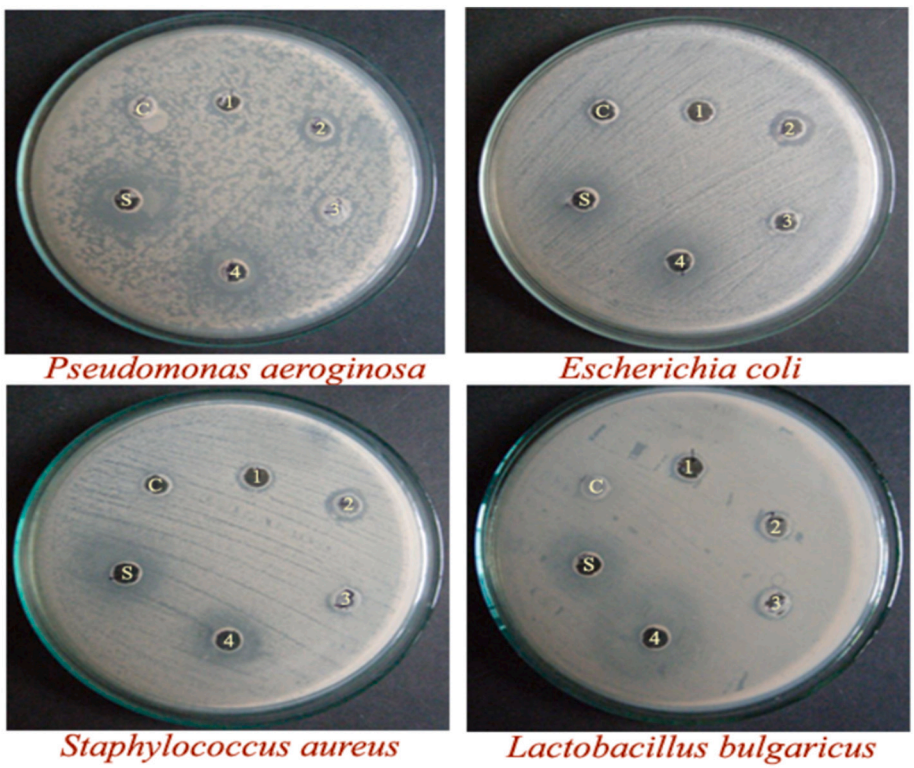

Fig. 7. Antibacterial studies of CH:F:SPG-CH:SNP against *Pseudomonas aeruginosa*, *Escherichia coli*, *Staphylococcus aureus* and *Lactobacillus bulgaricus* pathogens.

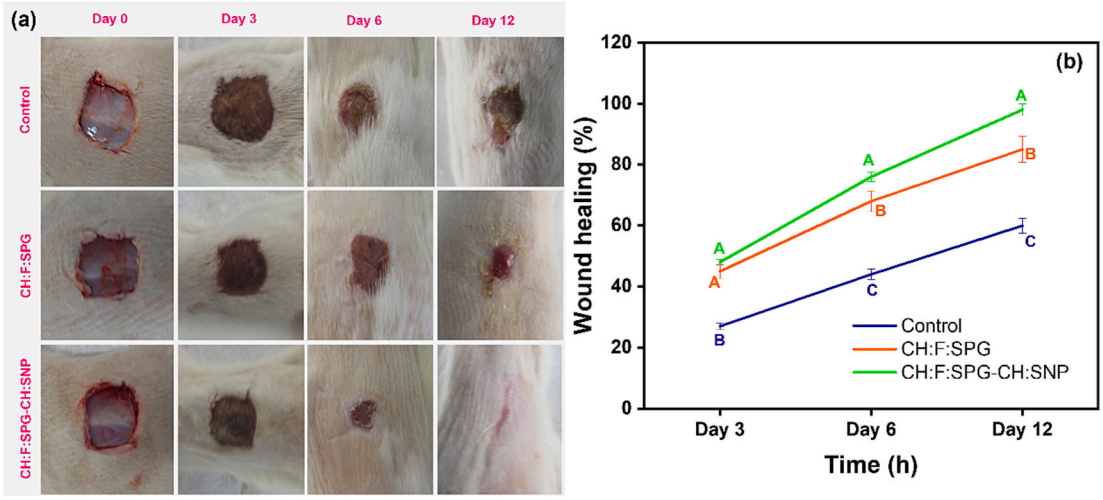

Fig. 8. (a) Photographic representation of wound contraction rate and (b) their wound healing rate. The error values are provided from the standard deviation of replicated experiments. Capital alphabets denote a significant deviation between the replicated experiments ($P \leq 0.05$).

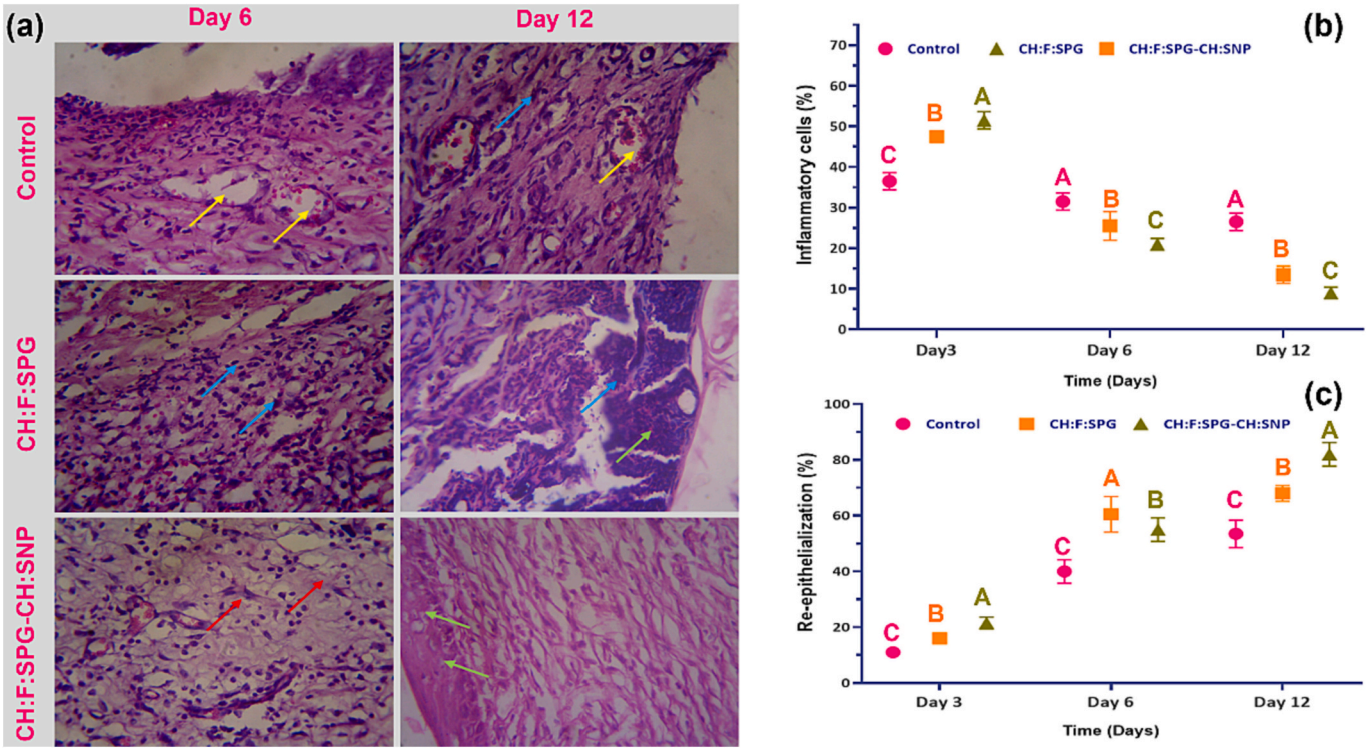

Fig. 9. (a) Histopathology studies using the CH:F:SPG-CH:SNP bandage (yellow arrow: congestion; blue arrow: hyperplasia; red arrow: granulocyte; green arrow: epithelial), (b) quantitative study of inflammatory cells (%) and (c) tissue re-epithelialization percentage (%) for control and treated with CH:F:SPG and CH:F:SPG-CH:SNP. The error values are provided from the standard deviation of replicated experiments. Capital alphabets denote a significant deviation between the replicated experiments ($P \leq 0.05$). (For interpretation of the references to colour in this figure legend, the reader is referred to the web version of this article.)

which demonstrates materials have improved healing mechanisms for the *in vivo* wound regenerations. The quantitative wound healing rate (%) observations was observed and demonstrated that SNP loaded bandage have fastening healing rate and achieved quicker epithelization when comparted to the control groups. Meanwhile, the wound healing mechanism was further observed by histological investigations by using H&E stain and microscopic technique to establish the process of fibroblast proliferations, re-epithelialization and inflammatory infiltrations. Fig. 9(a) displays the H&*E*-stained microscopic images of wound site for the control and after 6 and 12 days treated with prepared bandage materials. The observed image clearly describes the significant periods to healing wound site. Fig. 9(a) explores the considerable number of stained tissues for the CH:F:SPG-CH:SNP treated rat surface after 6 days due to the significant amount of infiltration of treated material. However, a control model owns more inflammatory cells than CH:F:SPG and CH:F:SPG-CH:SNP, which confirms that prepared wound bandages have provided a significant cure on the rat surface by infiltrations on inflammatory cells after 6 days. At the same time, CH:F:SPG-CH:SNP treated rat after 12 days shows the greater fibroblast proliferations, granulations tissues and specifically tissue re-epithelialization than the control and CH:F:SPG treated rat surface which ascertained the complete closure of wound during the periods. The inflammatory cells

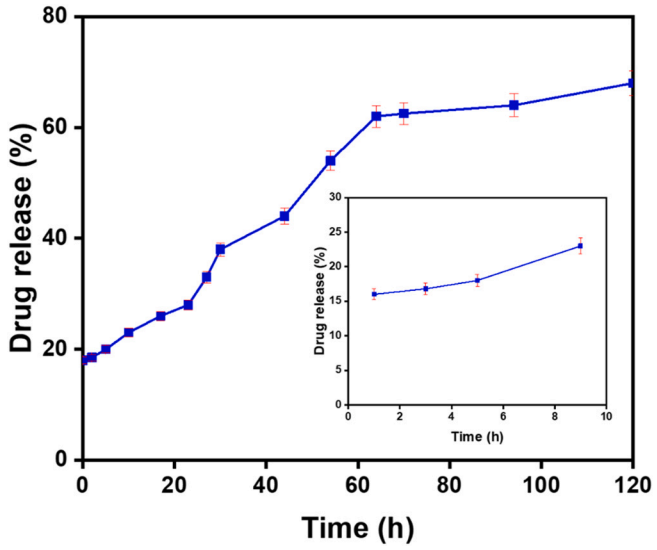

Fig. 10. *In vitro* drug release property of the CH:F:SPG-CH:SNP nanocomposites. The error values are provided from the standard deviation of replicated experiments.

infiltrations and tissue re-epithelialization rates were quantitatively measured as shown in Fig. 9(b) and (c), respectively. These results are extremely associated with previous microscopic and macroscopic observations of healing processes.

3.6. Drug release property

Drug release behavior of CH:F:SPG-CH:SNP nanocomposite is determined by *in vitro* with Franz diffusion cells (pH = 7.4). Fig. 10 shows the drug delivery properties of CH:F:SPG-CH:SNP framework for the sustained periods. Initially 15 % of released after an hour which indicates the promoted period at the wound surface from debris. Further, the drug release increases to 20 %, 40 % and 70 % at 10, 50 and 120 h, respectively which realizes the appropriate binding of drug with assembled framework. From the observed drug delivery results, the CH:F:SPG-CH:SNP is sustainable drug released material and it would ideal additive for the wound healing substitute. [58]

4. Conclusions

This work demonstrated the blend of chitosan coated SNPs and fibrin to produce a spongy like bandage framework by freeze drying technique for wound healing applications. The functional and surface properties were clearly confirmed in the formation of prepared composite framework model. Antibacterial studies estimated against *P. aeruginosa*, *E. coli, S. aureus* and L. *bulgaricus* pathogens by the zone inhibition model. Wound healing studies proved that use of CH:F:SPG-CH:SNP on open cutting out wounds could be cured faster rate with high biocompatibility. The derived hemolytic assay results enabled the stable safe substance of CH:F:SPG-CH:SNP for the human RBCs. *In vivo* studies realized the compatibility of prepared bilayer CH:F:SPG-CH:SNP bandage for real time use. The drug delivery studies clearly envisaged the drug release nature of prepared CH:F:SPG-CH:SNP framework. Hence, the development of CH:F:SPG-CH:SNP framework would be the potential candidate for wound healing and drug delivery applications.

CRediT authorship contribution statement

Anandhavelu Sanmugam: Conceptualization, Formal analysis, Methodology, Writing – original draft. **D. Shanthi:** Formal analysis. **Ananda Babu Sairam:** Investigation. **Raju Suresh Kumar:** Validation. **Abdulrahman I. Almansour:** Resources. **Natrajan Arumugam:** Validation. **A. Kavitha:** Data curation. **Hyun-Seok Kim:** Funding acquisition, Resources, Validation, Writing – review & editing. **Dhanasekaran Vikraman:** Investigation, Supervision, Validation, Writing – review & editing.

Declaration of competing interest

The authors declare that they have no known competing financial interests or personal relationships that could have appeared to influence the work reported in this paper.

Data availability

Data will be made available on request.

Acknowledgement

This work was partly supported by the Mid-career Researcher Program through the National Research Foundation of Korea (NRF) funded by the Ministry of Science and ICT (No. 2019R1A2C2086747). The authors extend their appreciation to the Deputyship for Research and Innovation, Ministry of Education, Saudi Arabia for funding this research work through the project number IFKSUOR3-488-2.

References

[1] S. Radin, T. Chen, P. Ducheyne, The controlled release of drugs from emulsified, sol gel processed silica microspheres, Biomaterials 30 (2009) 850–858.
[2] P. Kortesuo, M. Ahola, M. Kangas, T. Leino, S. Laakso, L. Vuorilehto, A. Yli-Urpo, J. Kiesvaara, M. Marvola, Alkyl-substituted silica gel as a carrier in the controlled release of dexmedetomidine, J. Control. Release 76 (2001) 227–238.
[3] H.U. Khan, F. Nasir, S. Maheen, S.S. Shafqat, S. Shah, A. Khames, M.M. Ghoneim, G. Abbas, S. Shabbir, M.A. Abdelgawad, M.A.S. Abourehab, A. Irfan, A.M. El Sisi, Antibacterial and wound-healing activities of statistically optimized nitrofurazone- and lidocaine-loaded silica microspheres by the Box-Behnken design, Molecules 27 (2022).
[4] K. Andiappan, A. Sanmugam, E. Deivanayagam, K. Karuppasamy, H.-S. Kim, D. Vikraman, Schiff base rare earth metal complexes: studies on functional, optical and thermal properties and assessment of antibacterial activity, Int. J. Biol. Macromol. 124 (2019) 403–410.
[5] W. Paul, C.P. Sharma, C. Tirunal, Chitosan and alginate wound dressings: a short review, Trends Biomater. Artif. Organs 18 (2004).
[6] P. Zahedi, I. Rezaeian, S.-O. Ranaei-Siadat, S.-H. Jafari, P. Supaphol, A review on wound dressings with an emphasis on electrospun nanofibrous polymeric bandages, Polym. Adv. Technol. 21 (2010) 77–95.
[7] S. Wang, W.-Y. Wu, J.C.C. Yeo, X.Y.D. Soo, W. Thitsartarn, S. Liu, B.H. Tan, A. Suwardi, Z. Li, Q. Zhu, X.J. Loh, Responsive hydrogel dressings for intelligent wound management, BMEMat 1 (2023), e12021.
[8] A. Ko, C. Liao, Hydrogel wound dressings for diabetic foot ulcer treatment: status-quo, challenges, and future perspectives, BMEMat 1 (2023), e12037.
[9] J.S. Boateng, K.H. Matthews, H.N.E. Stevens, G.M. Eccleston, Wound healing dressings and drug delivery systems: a review, J. Pharm. Sci. 97 (2008) 2892–2923.
[10] R.A.A. Muzzarelli, C. Muzzarelli, Chitosan chemistry: Relevance to the biomedical sciences, in: T. Heinze (Ed.), Polysaccharides I: Structure, Characterization and Use, Springer Berlin Heidelberg, Berlin, Heidelberg, 2005, pp. 151–209.
[11] K. Andiappan, A. Sanmugam, E. Deivanayagam, K. Karuppasamy, H.-S. Kim, D. Vikraman, In vitro cytotoxicity activity of novel Schiff base ligand–lanthanide complexes, Sci. Rep. 8 (2018) 3054.
[12] A.R. Ahmady, K. Razmjooee, S. Saber-Samandari, D. Toghraie, Fabrication of chitosan-gelatin films incorporated with thymol-loaded alginate microparticles for controlled drug delivery, antibacterial activity and wound healing: in-vitro and in-vivo studies, Int. J. Biol. Macromol. 223 (2022) 567–582.
[13] A. Sanmugam, L.K. Sellappan, S. Manoharan, A. Rameshkumar, R.S. Kumar, A. I. Almansour, N. Arumugam, H.-S. Kim, D. Vikraman, Development of chitosan-based cerium and titanium oxide loaded polycaprolactone for cutaneous wound healing and antibacterial applications, Int. J. Biol. Macromol. 256 (2024), 128458.
[14] R.G. Packirisamy, C. Govindasamy, A. Sanmugam, K. Karuppasamy, H.-S. Kim, D. Vikraman, Synthesis and antibacterial properties of novel $ZnMn_2O_4$–chitosan nanocomposites, Nanomaterials 9 (2019) 1589.
[15] J.J. Castellano, S.M. Shafii, F. Ko, G. Donate, T.E. Wright, R.J. Mannari, W. G. Payne, D.J. Smith, M.C. Robson, Comparative evaluation of silver-containing antimicrobial dressings and drugs, Int. Wound J. 4 (2007) 114–122.
[16] D. Pranantyo, K. Zhang, Z. Si, Z. Hou, M.B. Chan-Park, Smart multifunctional polymer systems as alternatives or supplements of antibiotics to overcome bacterial resistance, Biomacromolecules 23 (2022) 1873–1891.

[17] Z. Si, W. Zheng, D. Prananty, J. Li, C.H. Koh, E.-T. Kang, K. Pethe, M.B. Chan-Park, Polymers as advanced antibacterial and antibiofilm agents for direct and combination therapies, Chem. Sci. 13 (2022) 345–364.
[18] S. Anandhavelu, V. Dhanasekaran, V. Sethuraman, H.J. Park, Chitin and chitosan based hybrid nanocomposites for super capacitor applications, J. Nanosci. Nanotechnol. 17 (2017) 1321–1328.
[19] N. Ozmeriç, G. Ozcan, C.M. Haytaç, E.E. Alaaddinoğlu, M.F. Sargon, S. Senel, Chitosan film enriched with an antioxidant agent, taurine, in fenestration defects, J. Biomed. Mater. Res. 51 (2000) 500–503.
[20] N. Bhattarai, D. Edmondson, O. Veiseh, F.A. Matsen, M. Zhang, Electrospun chitosan-based nanofibers and their cellular compatibility, Biomaterials 26 (2005) 6176–6184.
[21] F. Karami, S. Saber-Samandari, Synthesis and characterization of a novel hydrogel based on carboxymethyl chitosan/sodium alginate with the ability to release simvastatin for chronic wound healing, Biomed. Mater. 18 (2023), 025001.
[22] K. Madhumathi, P.T. Sudheesh Kumar, S. Abhilash, V. Sreeja, H. Tamura, K. Manzoor, S.V. Nair, R. Jayakumar, Development of novel chitin/nanosilver composite scaffolds for wound dressing applications, J. Mater. Sci. Mater. Electron. 21 (2010) 807–813.
[23] L. Ma, C. Gao, Z. Mao, J. Zhou, J. Shen, X. Hu, C. Han, Collagen/chitosan porous scaffolds with improved biostability for skin tissue engineering, Biomaterials 24 (2003) 4833–4841.
[24] S.-Y. Ong, J. Wu, S.M. Moochhala, M.-H. Tan, J. Lu, Development of a chitosan-based wound dressing with improved hemostatic and antimicrobial properties, Biomaterials 29 (2008) 4323–4332.
[25] V. Thamilarasan, V. Sethuraman, K. Gopinath, C. Balalakshmi, M. Govindarajan, R. A. Mothana, N.A. Siddiqui, J.M. Khaled, G. Benelli, Single step fabrication of chitosan nanocrystals using Penaeus semisulcatus: potential as new insecticides, antimicrobials and plant growth promoters, J. Clust. Sci. 29 (2018) 375–384.
[26] R.G. Packirisamy, C. Govindasamy, A. Sanmugam, S. Venkatesan, H.-S. Kim, D. Vikraman, Synthesis of novel $Sn_{1-x}Zn_xO$-chitosan nanocomposites: structural, morphological and luminescence properties and investigation of antibacterial properties, Int. J. Biol. Macromol. 138 (2019) 546–555.
[27] V. Karthika, M.S. AlSalhi, S. Devanesan, K. Gopinath, A. Arumugam, M. Govindarajan, Chitosan overlaid Fe_3O_4/rGO nanocomposite for targeted drug delivery, imaging, and biomedical applications, Sci. Rep. 10 (2020) 18912.
[28] K. Vimala, Y.M. Mohan, K.S. Sivudu, K. Varaprasad, S. Ravindra, N.N. Reddy, Y. Padma, B. Sreedhar, K. MohanaRaju, Fabrication of porous chitosan films impregnated with silver nanoparticles: a facile approach for superior antibacterial application, Colloids Surf. B Biointerfaces 76 (2010) 248–258.
[29] C. Wang, S. Wang, D.D. Kang, Y. Dong, Biomaterials for in situ cell therapy, BMEMat 1 (2023), e12039.
[30] M.G.N. Campos, H.R. Rawls, L.H. Innocentini-Mei, N. Satsangi, In vitro gentamicin sustained and controlled release from chitosan cross-linked films, J. Mater. Sci. Mater. Med. 20 (2009) 537–542.
[31] C. Balalakshmi, N.S. Alharbi, S. Kadaikunnan, J.M. Khaled, K.F. Alanzi, K. Gopinath, A. Arumugam, M. Govindarajan, Development of chitosan/agar-silver nanoparticles-coated paper for antibacterial application, Green Process. Synth. 9 (2020) 751–759.
[32] J.M. Karp, F. Sarraf, M.S. Shoichet, J.E. Davies, Fibrin-filled scaffolds for bone-tissue engineering: an in vivo study, J. Biomed. Mater. Res. A 71A (2004) 162–171.
[33] T.A.E. Ahmed, E.V. Dare, M. Hincke, Fibrin: a versatile scaffold for tissue engineering applications, Tissue Eng. Part B Rev. 14 (2008) 199–215.
[34] L.J. Currie, J.R. Sharpe, R. Martin, The use of fibrin glue in skin grafts and tissue-engineered skin replacements: a review, Plast. Reconstr. Surg. 108 (2001).
[35] J.W. Weisel, Fibrinogen and Fibrin, Advances in Protein Chemistry, Academic Press, 2005, pp. 247–299.
[36] S. Cox, M. Cole, B. Tawil, Behavior of human dermal fibroblasts in three-dimensional fibrin clots: dependence on fibrinogen and thrombin concentration, Tissue Eng. 10 (2004) 942–954.
[37] L.-L. Chen, W.-P. Shi, T.-D. Zhang, W.-J. Lin, Y.-Q. Zhou, X.-Q. Jin, H. Liang, W.-H. Guo, D.-C. Yin, Synthesis of silver nanoparticles using lysozyme for scald-wound healing, ACS Appl. Nano Mater. 6 (2023) 17778–17791.
[38] V. Dhanasekaran, T. Mahalingam, Electrochemical and physical properties of electroplated CuO thin films, J. Nanosci. Nanotechnol. 13 (2013) 250–259.
[39] V. Dhanasekaran, T. Mahalingam, Physical properties evaluation of various substrates coated cupric oxide thin films by dip method, J. Alloys Compd. 539 (2012) 50–56.
[40] P. Singh, I. Mijakovic, Strong antimicrobial activity of silver nanoparticles obtained by the green synthesis in Viridibacillus sp. extracts, Front. Microbiol. 13 (2022).
[41] K. Ssekatawa, D.K. Byarugaba, C.D. Kato, E.M. Wampande, F. Ejobi, J. L. Nakavuma, M. Maaza, J. Sackey, E. Nxumalo, J.B. Kirabira, Green strategy–based synthesis of silver nanoparticles for antibacterial applications, Front. Nanotechnol. 3 (2021).
[42] A. Ahmed, M. Usman, Z. Ji, M. Rafiq, B. Yu, Y. Shen, H. Cong, Nature-inspired biogenic synthesis of silver nanoparticles for antibacterial applications, Mater. Today Chem. 27 (2023), 101339.
[43] M.A. Salami, F. Kaveian, M. Rafienia, S. Saber-Samandari, A. Khandan, M. Naeimi, Electrospun polycaprolactone/lignin-based nanocomposite as a novel tissue scaffold for biomedical applications, J. Med. Signals Sens. 7 (2017) 228–238.
[44] A. Anisiei, B.-I. Andreica, L. Mititelu-Tartau, C.G. Coman, R. Bilyy, G. Bila, I. Rosca, A.-I. Sandu, E. Amler, L. Marin, Biodegradable trimethyl chitosan nanofiber mats by electrospinning as bioabsorbable dressings for wound closure and healing, Int. J. Biol. Macromol. 249 (2023), 126056.
[45] J.W. Weisel, R.I. Litvinov, Fibrin formation, structure and properties, in: D.A. D. Parry, J.M. Squire (Eds.), Fibrous Proteins: Structures and Mechanisms, Springer International Publishing, Cham, 2017, pp. 405–456.
[46] G. Wechselberger, R.C. Russell, M.W. Neumeister, T. Schoeller, H. Piza-Katzer, C. Rainer, Successful transplantation of three tissue-engineered cell types using capsule induction technique and fibrin glue as a delivery vehicle, Plast. Reconstr. Surg. 110 (2002).
[47] D.J. Leaper, Silver dressings: their role in wound management, Int. Wound J. 3 (2006) 282–294.
[48] D. Pirone, J. Lim, F. Merola, L. Miccio, M. Mugnano, V. Bianco, F. Cimmino, F. Visconte, A. Montella, M. Capasso, A. Iolascon, P. Memmolo, D. Psaltis, P. Ferraro, Stain-free identification of cell nuclei using tomographic phase microscopy in flow cytometry, Nat. Photon. 16 (2022) 851–859.
[49] M. Son, Y.S. Lee, M.J. Lee, Y. Park, H.-R. Bae, S.Y. Lee, M.-G. Shin, S. Yang, Effects of osmolality and solutes on the morphology of red blood cells according to three-dimensional refractive index tomography, PloS One 16 (2022), e0262106.
[50] A. Gangwar, P. Kumar, R. Singh, P. Kush, Recent advances in mupirocin delivery strategies for the treatment of bacterial skin and soft tissue infection, Future Pharmacol. (2021) 80–103.
[51] X. Wang, Y. Du, H. Liu, Preparation, characterization and antimicrobial activity of chitosan–Zn complex, Carbohyd. Polym. 56 (2004) 21–26.
[52] A. Sanmugam, D. Vikraman, H.J. Park, H.S. Kim, One-pot facile methodology to synthesize chitosan-ZnO-graphene oxide hybrid composites for better dye adsorption and antibacterial activity, Nanomaterials 7 (2017) 363.
[53] S. Anandhavelu, S. Thambidurai, Single step synthesis of chitin/chitosan-based graphene oxide–ZnO hybrid composites for better electrical conductivity and optical properties, Electrochim. Acta 90 (2013) 194–202.
[54] N. Annabi, D. Rana, E. Shirzaei Sani, R. Portillo-Lara, J.L. Gifford, M.M. Fares, S. M. Mithieux, A.S. Weiss, Engineering a sprayable and elastic hydrogel adhesive with antimicrobial properties for wound healing, Biomaterials 139 (2017) 229–243.
[55] A. Sáenz-Trevizo, A.M. Hodge, Nanomaterials by design: a review of nanoscale metallic multilayers, Nanotechnology 31 (2020), 292002.
[56] A. Tripathi, J.S. Melo, Preparation of a sponge-like biocomposite agarose–chitosan scaffold with primary hepatocytes for establishing an in vitro 3D liver tissue model, RSC Adv. 5 (2015) 30701–30710.
[57] Z. Du, J. Liu, H. Zhang, B. Bao, R. Zhao, Y. Jin, Determination of hemolysis index thresholds for biochemical tests on Siemens Advia 2400 chemistry analyzer, J. Clin. Lab. Anal. 33 (2019), e22856.
[58] L.K. Sellappan, S. Anandhavelu, M. Doble, G. Perumal, J.-H. Jeon, D. Vikraman, H.-S. Kim, Biopolymer film fabrication for skin mimetic tissue regenerative wound dressing applications, Int. J. Polym. Mater. Polym. Biomater. 71 (2022) 196–207.